Bandgap Opening in Metallic Carbon Nanotubes Due to Silicon Adatoms

Branden B. Kappes [1] **and Cristian V. Ciobanu** [2]

Abstract: Controlling the bandgap of carbon nanostructures is a key factor in the development of mainstream applications of carbon-based nanoelectronic devices. This is particularly important in the cases where it is desired that the carbon nanostructures are the active elements, as opposed to being the conductive leads between other elements of the device. Here, we report density functional theory calculations of the effect of silicon impurities on the electronic properties of carbon nanotubes (CNTs). We have found that Si adatoms can open up a bandgap in intrinsically metallic CNTs, even when the linear density of Si atoms is low enough that they do not create an adatom chain along the tube. The bandgap opened in metallic CNTs can range up to approximately 0.47 eV, depending on adsorption site, on the linear density of Si adatoms, and on the chirality of the nanotube. We have found that a lower spatial symmetry of the charge transfer between adatom and CNT leads to a higher value of the bandgap opened, which indicates that the physical origin of the bandgap lies in the reduced spatial symmetry of the charge transferred.

Keywords: Carbon nanotubes, density functional theory, bandgap, electronic properties

1   Introduction

Much of the promise behind carbon nanotube-based electronic devices is fueled by the potential ability to control the electronic properties of materials systems with nanoscale dimensions. The high aspect ratio, strong covalent bonding, and long electron mean free path make CNTs ideal for ultra-thin interconnects; simultaneously, the ability to tune the electronic properties, such as the electronic bandgap, through physical [Dresselhaus and Avouris (2001a,b); Poklonski, Kislyakov, Hieu,

---

[1] Dept. of Mechanical Engineering, Colorado School of Mines, Golden, Colorado 80401, USA. Email: bkappes@mines.edu

[2] Dept. of Mechanical Engineering and Materials Science Program, Colorado School of Mines, Golden, Colorado 80401, USA. Email: cciobanu@mines.edu

Bubel', Vyrko, Popov and Lozovik (2008)] and chemical modifications [Rubio, Miyamoto, Blase, Cohen and Louie (1996); Zhang, Franklin, Chen and Dai (2000); Liu, Gao and Bando (2002)] provides a basis for creating versatile and novel nanoscale devices. Although the idea of bandgap engineering in CNTs is not new [Crespi, Cohen and Rubio (1997); Dresselhaus and Avouris (2001a); Yang, Zhao and Lu (2002); Miyake and Saito (2005)], realizing practical CNT-based devices is constrained by the lack of facile control over their electronic properties.

Chemical modification of CNTs via atoms adsorbed on them has a significant effect on their electronic properties, which can be understood through the impact that these adatoms can have in the first Brillouin zone (BZ) of the CNT. The BZ is a set of line segments whose separation and number are related to the CNT diameter, and whose length depends on spatial periodicity along the axis [Crespi, Cohen and Rubio (1997); Saito, Dresselhaus and Dresselhaus (1998)]. The BZ of a nanotube is rotated with respect to that of graphene by an angle related to the chirality of the nanotube. Ignoring the effects of the nanotube's curvature, the symmetry of the graphene and CNT reciprocal lattices permits the translation (folding) into the first BZ of graphene the line segments of the nanotube BZ. From this, it follows that a CNT will share those electronic properties of a graphene sheet that arise from their common symmetry points. Such is the origin of metallic, narrow- and broad-band gap semiconducting CNT; the BZ of the former passes through both the K and the K' of the graphene BZ, narrow-gap semiconductor CNT through the K point only, and broad-gap CNT through neither [Crespi, Cohen and Rubio (1997)]. Breaking the symmetry of a CNT using adatoms provides a mechanism for tailoring the electronic properties of these graphitic materials [Zhang, Franklin, Chen and Dai (2000); Li, Wang, Wei, Zhang, Xu, Luan, Wu and Wei (2002); Liu, Gao and Bando (2002); Zhang, Tang, Girit, Hao, Martin, Zettl, Crommie, Shen and Wang (2009)].

Investigations of the adsorption of various species has lead to the discovery of several new phenomena, including *semiconductor-to-metallic transitions* or functionality as spin polarizers for CNTs and graphene [Yang, Zhao and Lu (2002); Durgun, Dag, Bagci, Gulseren, Yildirim and Ciraci (2003); Lehtinen, Foster, Ayuela, Krasheninnikov, Nordlund and Nieminen (2003); Durgun, Dag, Ciraci and Gulseren (2004); Durgun and Ciraci (2006); Lehtinen, Foster, Ayuela, Vehvilainen and Nieminen (2004); Chan, Neaton and Cohen (2008); Mao, Yuan and Zhong (2008)]. As the efforts for carbon-based nanoelectronics develop in a technological climate that is still strongly dominated by silicon devices, it is useful to study the properties of nanostructures based on both carbon and silicon. Such studies can lead to novel applications based on tailoring the electronic properties of CNTs through doping with Si or binding with Si surfaces and nanostructures, as exemplified by the substitutional doping of CNTs with Si [Fagan, Mota, Da Silva and Fazzio (2004); Avramov,
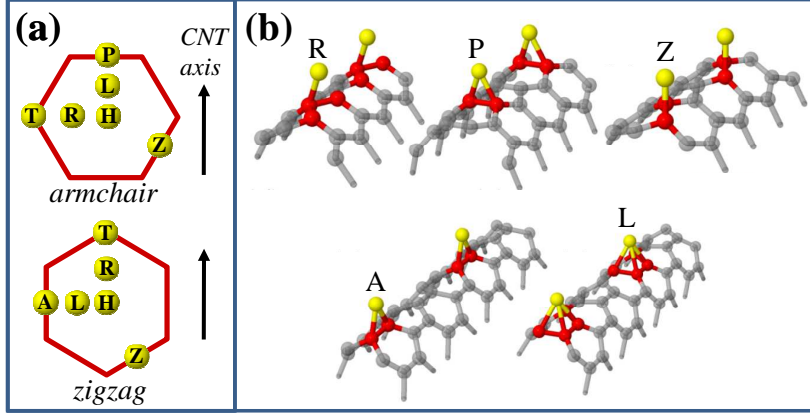
Figure 1: (a) Schematics of all possible starting positions of a Si adatom on CNTs. (b) Adatom positions preserved after full relaxation. For reference, R, P, and Z are the adatom configurations realized after relaxation in armchair CNTs, and A, L, R, and Z are the ones realized in zigzag CNTs.

Sorokin, Fedorov, Fedorov and Maeda (2006); Baierle, Fagan, Mota, da Silva and Fazzio (2001)] and by the interplay between CNT defects and adsorbed Si [da Silva, Fagan, Mota and Fazzio (2006)]. Here, we show that *metallic CNTs can become semiconducting* following Si atom adsorption, as opposed to substitution [Baierle, Fagan, Mota, da Silva and Fazzio (2001); Avramov, Sorokin, Fedorov, Fedorov and Maeda (2006)]. Even when the atomic concentration of adsorbed silicon is as low as 2%, *i.e.* lower than that necessary to form a bonded atomic chain along the nanotube, the doped CNT can develop a bandgap of up to 0.474 eV depending on the adsorption site, adatom density, and CNT chirality.

2   Computational Details

We have performed density functional theory (DFT) structural relaxations of CNT with adatoms. The computational cells in our DFT calculations contain a CNT with N unit cells along its axis and a single Si adatom which, before relaxation, can be located with respect to the CNT at the locations defined in Fig. 1(a). Figure 1(b) depicts cutouts of $N = 2$ repeated supercells for (5,5) CNTs (top) and (6,0) CNTs (bottom) at different initial locations of the Si adatom. The CNTs are labeled in our

work as $(n,m) \times N$, where N is the number of primitive cells along the tube axis in the supercell. We set vacuum spacings of 12 Å in the directions perpendicular to the axis. We performed DFT calculations using the generalized gradient approximation with VASP [Kresse and Furthmuller (1996a,b)] using the Perdew-Burke-Ernzerhof exchange-correlation functional [Perdew, Burke and Ernzerhof (1996)] and projector-augmented wave pseudopotentials [Kresse and Joubert (1999)]. The plane wave energy cut-off was set to 400 eV and the Brillouin zone was sampled using a $1 \times 1 \times 8$ Monkhorst-Pack grid for relaxations and a $1 \times 1 \times 48$ for band structure and density of states (DOS) calculations. All atoms were relaxed until each force component was smaller in magnitude than 0.01 eV/Å. A Gaussian broadening of 0.1 eV was applied. Although the correlation between CNT chirality and electronic properties is well established [Hamada, Sawada and Oshiyama (1992); Mintmire, Dunlap and White (1992); Saito, Fujita, Dresselhaus and Dresselhaus (1992); Miyake and Saito (2005)], we examine four CNTs of similar diameters: two armchair [(4,4) and (5,5)] and two zigzag [(6,0) and (7,0)] in an effort to isolate the properties that lead to the metallic to semiconductor transition. Both armchair CNTs are intrinsically metallic; (7,0) is semiconducting. Via the zone folding approach, the (6,0) CNT is predicted to be a narrow gap semiconductor, but $\sigma^* - \pi^*$ rehybridization render this tube metallic [Li, Xie, Zhou, Tang, Liu, Zou and Wang (2001); Dresselhaus and Avouris (2001a)].

Molecular dynamics (MD) simulations of various Si adatom-CNT systems were performed for 1.1 ns at 300, 600, 800, and 1000 K (canonical ensemble) using the simulation package LAMMPS [Plimpton (1995)]. The interactions between atoms were simulated using the Erhart-Albe parametrization [Erhart and Albe (2005)] of the Tersoff potential [Tersoff (1989)]. Silicon adatoms were placed 2.1 Å from a (5,5) SWCNT at one of the following six binding sites from Fig. 1: T, P, Z, R, L, H. Snapshots of atom positions, taken every 1 ps, were analyzed to determine the binding site and root mean square (RMS) displacement, taken with reference to the first snapshot at each temperature.

3 Results and Discussion

3.1 *Density Functional Theory*

Depending on the chirality of the CNT, the Si adatom relaxes preferentially over the P site, (*i.e.* above the midpoint of a C-C bond) on the armchair CNTs; on zigzag CNTs, the Si adatom binds preferentially over six-atom rings, *i.e.*, sites H, R, or L, (refer to Fig. 1). The binding energies for the selected CNTs and Si adatoms, along with the values of the electronic bandgap are summarized in Table 1, with the positive (negative) sign indicating that the bound (unbound) state of the adatom

is more energetically favorable than the unbound (bound) state. The binding energies that we calculated are somewhat lower than those reported elsewhere for larger diameter CNTs, but the stable binding sites are consistent with previous reports [Durgun, Dag, Bagci, Gulseren, Yildirim and Ciraci (2003); Lehtinen, Foster, Ayuela, Krasheninnikov, Nordlund and Nieminen (2003)]; it therefore appears that the preferred binding site is insensitive to the CNT diameter but not to chirality.

Table 1: Stability and electronic bandgap for selected CNTs doped with Si adatoms. The columns show the chiral vector (n,m), the Si spacing $d_{\text{Si-Si}}$, the two most stable sites with their binding energies E_b, the bandgap and the corresponding adatom position, and the number N of unit cells along the CNT.

(n,m)	$d_{\text{Si}-\text{Si}}$ (Å)	1st	E_b (eV)	2nd	E_b (eV)	Site, N	Gap (eV)
(4,4)	4.95	P	2.100	Z	1.786	R, 2	0.474
						Z, 2	0.259
	7.43	P	1.931	Z	1.694		
(5,5)	4.95	P	1.219	Z	1.200	R, 2	0.428
						Z, 2	0.235
	7.43	Z	1.424	R	1.363		
(6,0)	4.29	R	2.179	Z	1.785	R, 1	0.290
	8.58	L	2.377	Z	2.226		
	12.9	Z	2.249	A	1.978		
(7,0)	8.58	L	2.120	Z	2.021	A, 2	0.402
						Z, 2	0.352
						L, 2	0.304
	12.9	Z	-1.998	A	-1.584	A, 3	0.356
						Z, 3	0.319

Table 1 further clarifies the relationship between the chirality of the CNT and the most stable binding site for Si. On the (4,4) CNT, the Si adatom breaks the highly strained, P-site C–C bond to form two, 1.9 Å long Si–C bonds; the formation of such a "bridge" is consistent with previous reports [Lehtinen, Foster, Ayuela, Vehvilainen and Nieminen (2004)]. The binding energy of Si on the (5,5) CNT is

substantially smaller, despite the increased tube diameter, because the P-site C–C bond is not broken and therefore no strain is released. Lacking a transverse C–C bond, the Si adatoms on the (6,0) and (7,0) zigzag CNTs tend toward one of the three sites inside a six-carbon ring (H, L, or R), and display a larger binding energy [Durgun, Dag, Bagci, Gulseren, Yildirim and Ciraci (2003); Lehtinen, Foster, Ayuela, Vehvilainen and Nieminen (2004)] than the adatoms on the (5,5) armchair tube. It is interesting to note that the preferred adatom site depends on the linear density of Si atoms; with the exception of the (4,4) nanotube, the two most stable sites on the selected CNTs change with the distance between the adatoms (refer to Table 1). This observation shows that despite low linear adatom densities (< 2 Si atoms/nm) and the absence of a bonded adatom chain along the CNT, there are still significant strain-mediated interactions between adatoms.

The binding of Si adatoms to CNTs and the tube-mediated interactions that occur for densities lower than 2 adatoms/nm are responsible for altering the electronic properties of CNTs. Binding at certain sites is accompanied by the opening of a bandgap in intrinsically metallic CNTs, reaching values of 0.474 eV. Adsorption at site R induces a bandgap for the metallic tubes studied here (Table 1) provided that the distance between adatom images along the CNT (*i.e.*, the periodic length along the tube) remains smaller than 5 Å. This is particularly interesting for the (6,0) case, where the most stable adsorption site (R) is the only one that leads to a significant electronic gap (0.29 eV). The Si adatoms also affect the electronic structure of the semiconducting (7,0) tube, which in the absence of impurities, has a gap of 0.233 eV; as seen in the Table 1, adsorption at sites A, Z, or L increases this gap beyond 0.3 eV.

To better illustrate the influence of Si adatoms on metallic CNTs, we plot, in Fig. 2(a,b), the electronic band structure and density of states of Si-doped (5,5) CNTs for two adsorption sites (R and Z) in comparison to those of the same CNT without adatoms. For both sites, adsorption of Si leads to significant band splitting, band bending, and heavy bands around the Fermi level, which ultimately determine the bandgap of the doped CNTs. While the band structures in Figs. 2(a) and (b) show gaps of 0.428 eV and 0.235 eV, respectively, in the DOS plots these values appear somewhat smaller due to Gaussian smearing.

For the same (5,5) CNT and with the same linear density of Si adatoms, we plot the isosurfaces of electron density transferred upon adsorption of silicon at sites R, Z, and P [see Fig. 2(c)]. The transferred electron density $\Delta\rho(\mathbf{r})$ is defined here as the difference between the electronic density of the doped system $\rho_{CNT+Si}(\mathbf{r})$, the electron density of the pure nanotube $\rho_{CNT}(\mathbf{r})$, and the lone adatom $\rho_{Si}(\mathbf{r})$:

$$\Delta\rho(\mathbf{r}) \equiv \rho_{CNT+Si}(\mathbf{r}) - \rho_{CNT}(\mathbf{r}) - \rho_{Si}(\mathbf{r}). \tag{1}$$
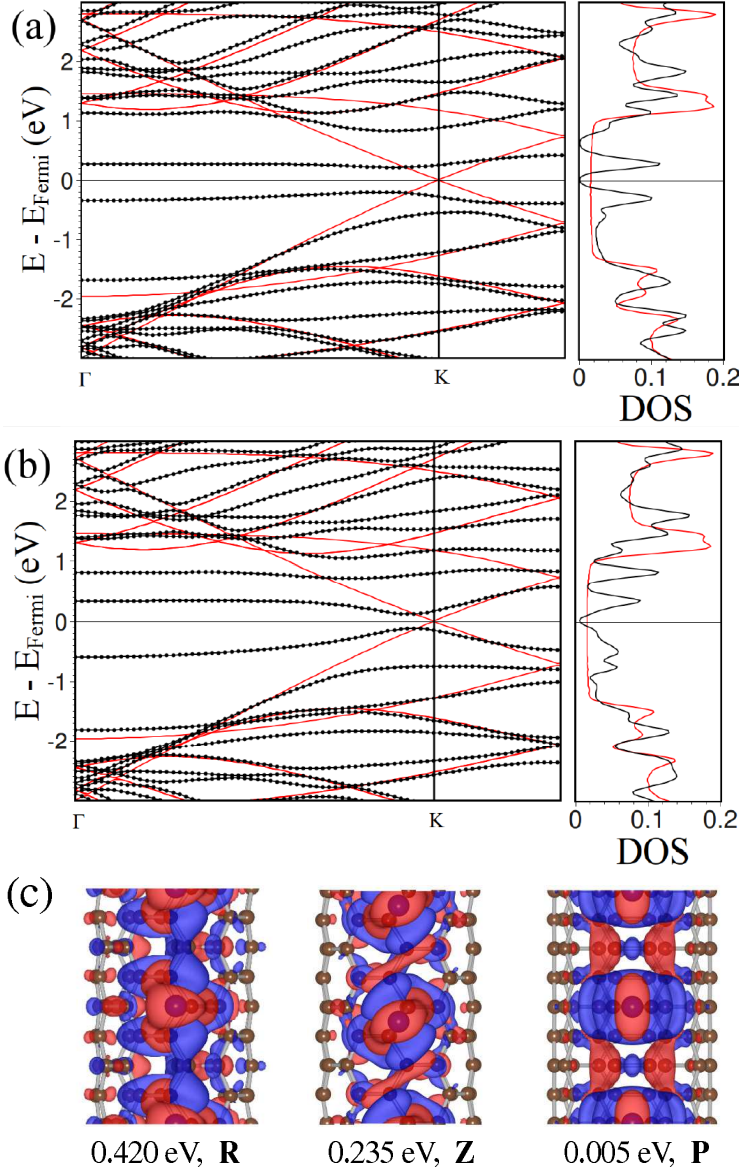
Figure 2: (a,b) Band structure (left) and density of states (DOS, right) for a (5,5) CNT with $N = 2$ and the Si adatom placed at (a) site R and (b) site Z. The continuous red lines with no markers show the band structure and DOS for the (5,5) tube with no adatoms (*i.e.*, undoped). (c) Isosurfaces of the charge density transfer (red excess, blue deficit) for the (5,5) CNT with Si adatom at R, Z, and P sites, showing the correlation between the increased spatial symmetry of the electron transfer and the decrease of the bandgap.

Depending on the adsorption site, the charge transfer displays different symmetries. When the symmetry group of the transferred density is C_s (site R) the gap is 0.42 eV, but as seen in Fig. 2(c), the value of the bandgap decreases with increasing charge transfer symmetry; in the case of site P, the bandgap is virtually absent. We have found this correlation between the bandgap value and the symmetry of transferred charge density for each metallic nanotube that we investigated, and we have illustrated it in Fig. 3. The high-symmetry regions of depleted (blue) and augmented (red) charge densities that exist when Si is located at the P or A sites inhibit the formation of a band gap, *e.g.* those systems that have C_{2v} space group symmetry, as seen in the last row in Fig. 3. Conversely, atoms at the R and L sites (which lead to C_1 and C_s symmetry groups of the spatial charge transfer) reveal a disparity in the charge density at the two carbon sublattices of the CNT; such asymmetry leads to the largest bandgaps (see top three rows of Fig. 3). Bandgap opening originating from breaking the symmetry between the two sublattices that form the nanotube has also been encountered in epitaxial graphene [Zhou, Gweon, Fedorov, First, De Heer, Lee, Guinea, Neto and Lanzara (2007); Kwon, Ciobanu, Petrova, Shenoy, Bareno, Gambin, Petrov and Kodambaka (2009)]. We have also verified that the correlation between the value of the bandgap opened in metallic nanotubes and the spatial symmetry of the electronic transfer exists for a much more obvious type of symmetry breaking, *i.e.* that in which the Si atom substitutes one carbon atom of the nanotube. In this case, for impurity spacings similar to those shown in Table 1, the bandgap values are ~ 0.15 eV (which are smaller than the most of the values reported in Table 1), which suggests that adsorbed atoms are more effective in opening a bandgap in metallic CNTs than the substitutional ones at the same linear density. This result is consistent with a recent report on bandgap opening via substitutional Si atoms on (8,8) nanotubes Avramov, Sorokin, Fedorov, Fedorov and Maeda (2006).

While we have found that Si adatoms can induce metallic to semiconductor transitions in CNTs, the question remains whether CNTs with active Si adsorbates are thermodynamically accessible, and, furthermore, if the adatom sites that lead to opening a bandgap are populated for sufficiently long times to actually affect the electronic properties of metallic CNTs.

3.2 *Molecular Dynamics*

Similarities between diffusion behavior in graphene and CNTs suggest that procedures to control adatom concentrations on graphene by standard processes may also be applicable to CNTs [Lehtinen, Foster, Ayuela, Krasheninnikov, Nordlund and Nieminen (2003); Banhart (1999)]. From Table 1, assuming a low-flux random deposition of Si adatoms, both the (6,0) and (5,5) CNT would realize a large num-
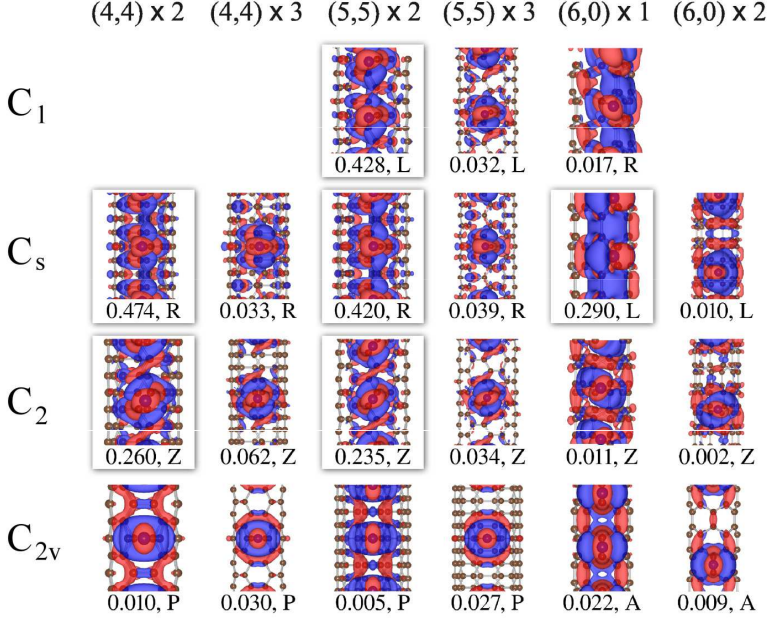
Figure 3: Relationship between the occurrence of electronic bandgaps (value in eV given below each panel, along with the adatom site) and the charge transfer upon Si doping of intrinsically metallic CNTs (isosurface plots at ± 0.001 electrons/$\text{\AA}^3$). The formation of a significant bandgap in certain structures (framed, with drop shadow) depends on the CNT curvature, the binding site of the Si adatom, and the linear density of adatoms ($\propto 1/N$). The spatial symmetry of the charge transfer provides additional insight into the trend of Si-doped metallic CNTs to form a bandgap: the higher the symmetry of $\Delta\rho$, the smaller the value of the bandgap. The high-symmetry regions of depleted (blue) and augmented (red) charge densities that exist when Si is located at the P or A sites inhibit the formation of a band gap, *e.g.* those systems that are in the C_{2v} space group, the bottom row. Conversely, atoms at the R and L sites, those with C_1 or C_s space group symmetries of the charge transfer, reveal a disparity in the charge density at the two carbon sublattices of the CNT and lead to the largest bandgaps.

ber of Si adatoms at sites that can induce the metallic to semiconductor transition, the former populating over 90% of these sites below 1500 K –a soft upper limit for temperatures achieved on common heating stages [Banhart (1999)]. As mentioned, we performed canonical ensemble MD simulations for four different temperatures.

After 1.1 ns, we have analyzed the populations of different types of binding sites. Often, the types of site can be determined by the distances from the adatom to its neighboring atoms on the nanotube. The results of this binding site analysis are summarized in Fig. 4. Each of the six binding sites for armchair nanotubes have a unique neighbor "signature", for example, the top site, T, has one neighbor at the Si–C bond length ($d_{\text{Si–C}}$), three at $\sqrt{d_{\text{Si–C}}^2 + d_{\text{C–C}}^2}$, *etc.* Using this method, approximately 60% of adsorbed atom positions can be unambiguously identified.
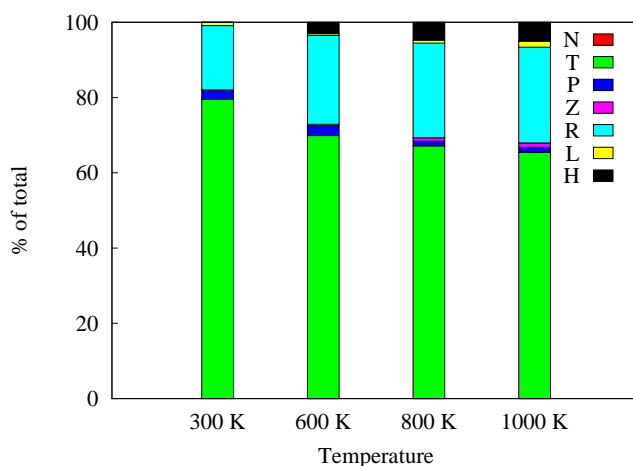

Figure 4: Binding site populations for those atoms whose binding site could be determined by neighbor bond length analysis at 300, 600, 800, and 1000 K. Although predominantly found at T sites, up to 25% of adsorbed silicon bonds at the R site; the site shown to open a 0.47 eV band gap in the (5,5) SWCNT.

Fig. 4 reveals that a significant population of silicon atoms are adsorbed at R sites. Although the T site is the one that is the most populated and not R, the R site still has significant occupancy and is the site where adsorption of Si leads to an electronic bandgap (Table 1). When compared to Table 1, the results of Figure 4 suggest a change in the relative stability of the binding sites as compared to that predicted by our zero Kelvin DFT calculations. This is an artifact of the Earhart-Albe interatomic potential used in the MD simulations, but would most likely appear for all the empirical potentials that were not designed or parameterized specifically for Si adatom-CNT configurations –such as, *e.g.*, the original Tersoff potential [Tersoff (1989)], or more complex potentials such as reactive force fields [van Duin, Dasgupta, Lorant and Goddard (2001); Narayanan, van Duin, Kappes, Reimanis and Ciobanu (2012)]. The population of R sites, increasing to 25% at 1000 K, is espe-
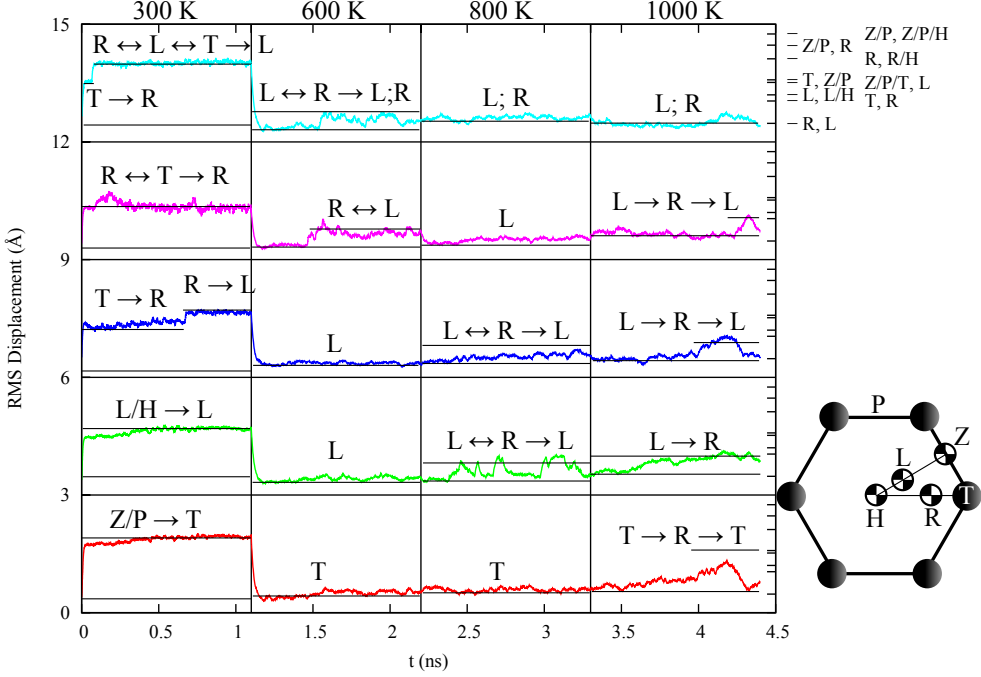
Figure 5: Root mean square displacement exponentially weighted over time for five randomly selected silicon adatoms at 300 K (0–1.1 ns), 600 K (1.1–2.2 ns), 800 K (2.2–3.3 ns), and 1000 K (3.3–4.4 ns). The RMS deviation is taken with reference to the first snapshot at each temperature. The reference for 300 K is the original, randomly assigned binding site. Arrows indicate transitions between binding configurations; semicolons indicate an uncertainty in the location of the binding site. In the text, references are made curves both by color and by number, starting with the bottom curve (numbered 1). The schematic (bottom right) shows one-sixth of the binding sites projected onto a planar six-atom ring. The right axis tic labels are the distances between binding sites, *i.e.* "R, L", drawn at 0.21 Å, is the distance separating the nearest R and L sites.

cially fortuitous as silicon adsorption at this site is shown to open a 0.428 eV band gap.

We have also analyzed the transition of adatoms from one binding site to another by plotting their RMS displacement, as shown in Fig. 5. We compared the observed transitions (jumps in the RMS) to the calculated distance between binding sites in which we accounted for the Si–C bond lengths. Transitions between binding sites occur either as discontinuous jumps, as seen at ∼2.4 ns in the green (second) curve

in Fig. 5, or as diffusive migrations, such as that shown in the 3.5–4.2 ns time interval of the red (first) curve (Fig. 5).

The determination of the RMS displacements takes into account the periodic translations along the SWCNT axis and the possible motion of the center of mass of the nanotube. The results shown in Fig. 5 are obtained for five randomly selected silicon adatoms. The red line (lowermost graph) in Fig. 5 shows that this adatom originally moved from a P or Z site to a T site, where it remained until heated to 1000 K at which temperature it begins to drift toward an R site. These five data sets reveal that distinct transitions occur regularly, but the absence of the square-root-of-time dependence associated with diffusive migration suggests that the adsorbed silicon remain stable at a number of binding sites.

The magenta curve (fourth graph from the bottom) in Fig. 5 oscillates rapidly between the initial T and R sites. Similarly, between 1.5 and 2.2 ns at 600 K, the magenta curve oscillates rapidly between the R and L sites; however, because the adatom bound at 300 K must be at either R or T, the initial position at 600 K (1.1 ns) must be one of these two. From that site, an R to L transition must be possible, so the adatom must have settled at the R site at 300 K to allow for a transition to the L site during the 600 K anneal. Identifying the remaining transitions of this and the other RMS curves follows a similar logic.

Qualitatively, observation of the dynamic Si–Si and Si–C bond formation and bond breaking reveals an approximate parity between the bonding preference at various temperatures for silicon adsorbed on a (5,5) CNT. Therefore, silicon cluster formation depends on the initial deposition method since stable Si–Si and Si–C bonding may lead to immobile adsorbates.

4   Concluding Remarks

In conclusion, we have shown evidence that adsorbed silicon impurities with atomic concentrations as low as ∼2% can induce a bandgap in intrinsically metallic CNTs, and can also modify the bandgap of semiconducting CNTs. Our work, which differs from previous reports [*e.g.* Baierle, Fagan, Mota, da Silva and Fazzio (2001); Fagan, Mota, Da Silva and Fazzio (2004); Avramov, Sorokin, Fedorov, Fedorov and Maeda (2006)] in its focus on adatoms rather than on substitutional impurities, distinguishes between the structural and electronic asymmetries that impact the two carbon sublattices, describes how this asymmetry may be identified, and how a bandgap can be opened via Si adsorption. The value of the induced gap depends on the adatom density, adsorption site, and nanotube chirality: the higher the symmetry of the charge transfer the lower the value of the induced bandgap. These results may be useful in integrating CNTs with Si-based devices; for example, en-

gineering the CNT bandgap by careful epitaxial arrangement of CNTs on silicon surfaces selected to form Si–C bonds at prescribed intervals.

References

Avramov, P. V.; Sorokin, P. B.; Fedorov, A. S.; Fedorov, D. G.; Maeda, Y. (2006): Band-gap unification of partially Si-substituted single-wall carbon nanotubes. *Physical Review B*, vol. 74, Art. no. 245417.

Baierle, R.; Fagan, S.; Mota, R.; da Silva, A.; Fazzio, A. (2001): Electronic and structural properties of silicon-doped carbon nanotubes. *Physical Review B*, vol. 64, Art. no. 085413.

Banhart, F. (1999): Irradiation effects in carbon nanostructures. *Reports on Progress in Physics*, vol. 62, pp. 1181–1221.

Chan, K. T.; Neaton, J. B.; Cohen, M. L. (2008): First-principles study of metal adatom adsorption on graphene. *Physical Review B*, vol. 77, Art. no. 235430.

Crespi, V.; Cohen, M.; Rubio, A. (1997): In situ band gap engineering of carbon nanotubes. *Physical Review Letters*, vol. 79, pp. 2093–2096.

da Silva, L. B.; Fagan, S. B.; Mota, R.; Fazzio, A. (2006): Silicon adsorption in defective carbon nanotubes: a first principles study. *Nanotechnology*, vol. 17, pp. 4088–4091.

Dresselhaus, M.; Avouris, P. (2001): Introduction to carbon materials research. In *Carbon Nanotubes*, volume 80 of *Topics in Applied Physics*, pp. 113–145. Springe-Verlag, Berlin, Germany.

Dresselhaus, M.; Avouris, P. (2001): Introduction to carbon materials research. In *Carbon Nanotubes*, volume 80 of *Topics in Applied Physics*, pp. 147–171. Springer-Verlag, Berlin, Germany.

Durgun, E.; Ciraci, S. (2006): Spin-dependent electronic structure of transition-metal atomic chains adsorbed on single-wall carbon nanotubes. *Physical Review B*, vol. 74, Art. no. 125404.

Durgun, E.; Dag, S.; Bagci, V.; Gulseren, O.; Yildirim, T.; Ciraci, S. (2003): Systematic study of adsorption of single atoms on a carbon nanotube. *Physical Review B*, vol. 67, Art. no. 235430.

Durgun, E.; Dag, S.; Ciraci, S.; Gulseren, O. (2004): Energetics and electronic structures of individual atoms adsorbed on carbon nanotubes. *Journal of Physical Chemistry B*, vol. 108, pp. 575–582.

Erhart, P.; Albe, K. (2005): Analytical potential for atomistic simulations of silicon, carbon, and silicon carbide. *Physical Review B*, vol. 71, Art. No. 035211.

Fagan, S.; Mota, R.; Da Silva, A.; Fazzio, A. (2004): Substitutional Si doping in deformed carbon nanotubes. *Nano Letters*, vol. 4, pp. 975–977.

Hamada, N.; Sawada, S.; Oshiyama, A. (1992): New One-dimensional Conductors - Graphitic Microtubules. *Physical Review Letters*, vol. 68, pp. 1579–1581.

Kresse, G.; Furthmuller, J. (1996): Efficiency of ab-initio total energy calculations for metals and semiconductors using a plane-wave basis set. *Computational Materials Science*, vol. 6, pp. 15–50.

Kresse, G.; Furthmuller, J. (1996): Efficient iterative schemes for ab initio total-energy calculations using a plane-wave basis set. *Physical Review B*, vol. 54, pp. 11169–11186.

Kresse, G.; Joubert, D. (1999): From ultrasoft pseudopotentials to the projector augmented-wave method. *Physical Review B*, vol. 59, pp. 1758–1775.

Kwon, S.-Y.; Ciobanu, C. V.; Petrova, V.; Shenoy, V. B.; Bareno, J.; Gambin, V.; Petrov, I.; Kodambaka, S. (2009): Growth of Semiconducting Graphene on Palladium. *Nano Letters*, vol. 9, pp. 3985–3990.

Lehtinen, P.; Foster, A.; Ayuela, A.; Krasheninnikov, A.; Nordlund, K.; Nieminen, R. (2003): Magnetic properties and diffusion of adatoms on a graphene sheet. *Physical Review Letters*, vol. 91, Art. no. 017202.

Lehtinen, P.; Foster, A.; Ayuela, A.; Vehvilainen, T.; Nieminen, R. (2004): Structure and magnetic properties of adatoms on carbon nanotubes. *Physical Review B*, vol. 69, Art. no. 155422.

Li, Y.; Wang, S.; Wei, J.; Zhang, X.; Xu, C.; Luan, Z.; Wu, D.; Wei, B. (2002): Lead adsorption on carbon nanotubes. *Chemical Physics Letters*, vol. 357, pp. 263–266.

Li, Y.; Xie, S.; Zhou, W.; Tang, D.; Liu, Z.; Zou, X.; Wang, G. (2001): Small diameter carbon nanotubes synthesized in an arc-discharge. *Carbon*, vol. 39, pp. 1429–1431.

Liu, Z.; Gao, Y.; Bando, Y. (2002): Highly effective metal vapor absorbents based on carbon nanotubes. *Applied Physics Letters*, vol. 81, pp. 4844–4846.

Mao, Y.; Yuan, J.; Zhong, J. (2008): Density functional calculation of transition metal adatom adsorption on graphene. *Journal of Physics: Condensed Matter*, vol. 20, Art. no. 115209.

Mintmire, J.; Dunlap, B.; White, C. (1992): Are Fulerene Tubules Metallic? *Physical Review Letters*, vol. 68, pp. 631–634.

Miyake, T.; Saito, S. (2005): Band-gap formation in (n,0) single-walled carbon nanotubes (n=9,12,15,18): A first-principles study. *Physical Review B*, vol. 72, Art. no. 073404.

Narayanan, B.; van Duin, A. C. T.; Kappes, B. B.; Reimanis, I. E.; Ciobanu, C. V. (2012): A reactive force field for lithium-aluminum silicates with applications to eucryptite phases. *Modelling and Simulation in Materials Science and Engineering*, vol. 20, Art. no. 015002.

Perdew, J.; Burke, K.; Ernzerhof, M. (1996): Generalized gradient approximation made simple. *Physical Review Letters*, vol. 77, pp. 3865–3868.

Plimpton, S. (1995): Fast Parallel Algorithms for Short-Range Molecular Dynamics. *Journal of Computational Physics*, vol. 117, pp. 1–19.

Poklonski, N. A.; Kislyakov, E. F.; Hieu, N. N.; Bubel', O. N.; Vyrko, S. A.; Popov, A. M.; Lozovik, Y. E. (2008): Uniaxially deformed (5,5) carbon nanotube: Structural transitions. *Chemical Physics Letters*, vol. 464, pp. 187–191.

Rubio, A.; Miyamoto, Y.; Blase, X.; Cohen, M.; Louie, S. (1996): Theoretical study of one-dimensional chains of metal atoms in nanotubes. *Physical Review B*, vol. 53, pp. 4023–4026.

Saito, R.; Dresselhaus, G.; Dresselhaus, M. (1998): *Physical Properties of Carbon Nanotube*. Imperial College Press.

Saito, R.; Fujita, M.; Dresselhaus, G.; Dresselhaus, M. (1992): Electronic Structure of Graphene Tubules Based on C_{60}. *Physical Review B*, vol. 46, pp. 1804–1811.

Tersoff, J. (1989): Modeling solid-state chemistry: Interatomic potentials for multicomponent systems. *Physical Review B*, vol. 39, pp. 5566–5568.

van Duin, A.; Dasgupta, S.; Lorant, F.; Goddard, W. (2001): ReaxFF: A reactive force field for hydrocarbons. *Journal of Physical Chemistry A*, vol. 105, pp. 9396–9409.

Yang, C.; Zhao, J.; Lu, J. (2002): Binding energies and electronic structures of adsorbed titanium chains on carbon nanotubes. *Physical Review B*, vol. 66, Art. no. 041403.

Zhang, Y.; Franklin, N.; Chen, R.; Dai, H. (2000):   Metal coating on suspended carbon nanotubes and its implication to metal-tube interaction. *Chemical Physics Letters*, vol. 331, pp. 35–41.

Zhang, Y.; Tang, T.-T.; Girit, C.; Hao, Z.; Martin, M. C.; Zettl, A.; Crommie, M. F.; Shen, Y. R.; Wang, F. (2009):   Direct observation of a widely tunable bandgap in bilayer graphene. *Nature*, vol. 459, pp. 820–823.

Zhou, S. Y.; Gweon, G.-H.; Fedorov, A. V.; First, P. N.; De Heer, W. A.; Lee, D.-H.; Guinea, F.; Neto, A. H. C.; Lanzara, A. (2007):   Substrate-induced bandgap opening in epitaxial graphene. *Nature Materials*, vol. 6, pp. 770–775.